Article

Fast-Recoverable, Self-Healable, and Adhesive Nanocomposite Hydrogel Consisting of Hybrid Nanoparticles for Ultrasensitive Strain and Pressure Sensing

Xiaohui Yu, Yong Zheng, Haopeng Zhang, Yufei Wang, Xiaoshan Fan,* and Tianxi Liu*

Read Online

ACCESS | Metrics & More | Article Recommendations | SI Supporting Information

AAc   PAA polymer chain   PAA/SiO$_2$-g-PAAm   Dynamic hydrogen bonding
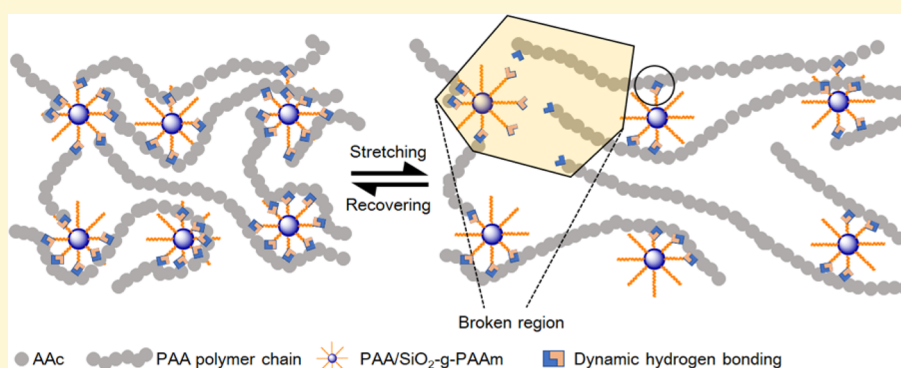
ABSTRACT: To meet various practical requirements and enhance human experience, hydrogels possessing multifunctionality are of great significance for flexible wearable sensors. Herein, a novel strategy has been developed to fabricate nanocomposite hydrogels with a combination of excellent stretchability, rapid recoverability, self-healing, and outstanding adhesiveness. The PAAc/SiO$_2$-g-PAAm nanocomposite hydrogels were facilely prepared through the polymerization of acrylic acid (AAc) using SiO$_2$-g-polyacrylamide core−shell hybrid nanoparticles (SiO$_2$-g-PAAm) as the dynamic cross-linking center. The densely dynamic hydrogen bonds between PAAc matrices and grafted PAAm chains could reversibly be destructed and reconstructed to dissipate a large amount of energy. Due to this unique feature, the formulated hydrogels showed a wide spectrum of desirable properties, including skin-mimetic modulus, excellent stretchability (1600%), exceptional self-healing properties (96.5% at ambient temperature), and fast recoverability. The sensors fabricated with the prepared hydrogels exhibited a high detection sensitivity in the strain range from 50% to 500% with a gauge factor value of 5.86, rapid response time, and good antifatigue performance. Depending on the outstanding adhesiveness, this sensor could attach to different substrates to release the real-time motion monitoring. In the practical wearable sensing test, various human motions, including tiny-scaled swallowing, laughing, and speaking, as well as large-scaled wrist, elbow, and knee movements during basketball shooting, could be sensed. These demonstrations heralded the potential application of our sensor in accurate and long-term human motion monitoring.

1. INTRODUCTION

Flexible and wearable electric devices have been attracting dramatic attention from materials scientists due to their potential applications for human−machine interfaces, personal healthcare diagnosis, and activity monitoring.[1−5] They are capable of monitoring external stimuli such as pressure,[6,7] strain,[8−10] and temperature[11] and further convert them into electrical signals in accordance with various deformations. Hydrogels are three-dimensional (3D) networks composed of cross-linked hydrophilic polymers with substantial amounts of water.[12−16] Due to their biocompatibility and extraordinary softness, hydrogels show great potential in wearable sensors.[17] However, conventional hydrogels are usually fragile and weak and may readily break upon stretching because of their poor mechanical properties, thus limiting their practical applications.

In addition, most of the hydrogels suffer from a lack of self-healing capability, which is significantly important for hydrogel biosensors to prolong their life spans and enhance their reliability.[18−22] Furthermore, the hydrogel-based biosensors without adhesiveness are attached onto the body utilizing tapes or belts, leading to the poor signal capture ability and bad human experience.[23−29] Therefore, hydrogels integrated with decent mechanical strength, self-healing, and adhesiveness
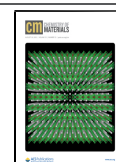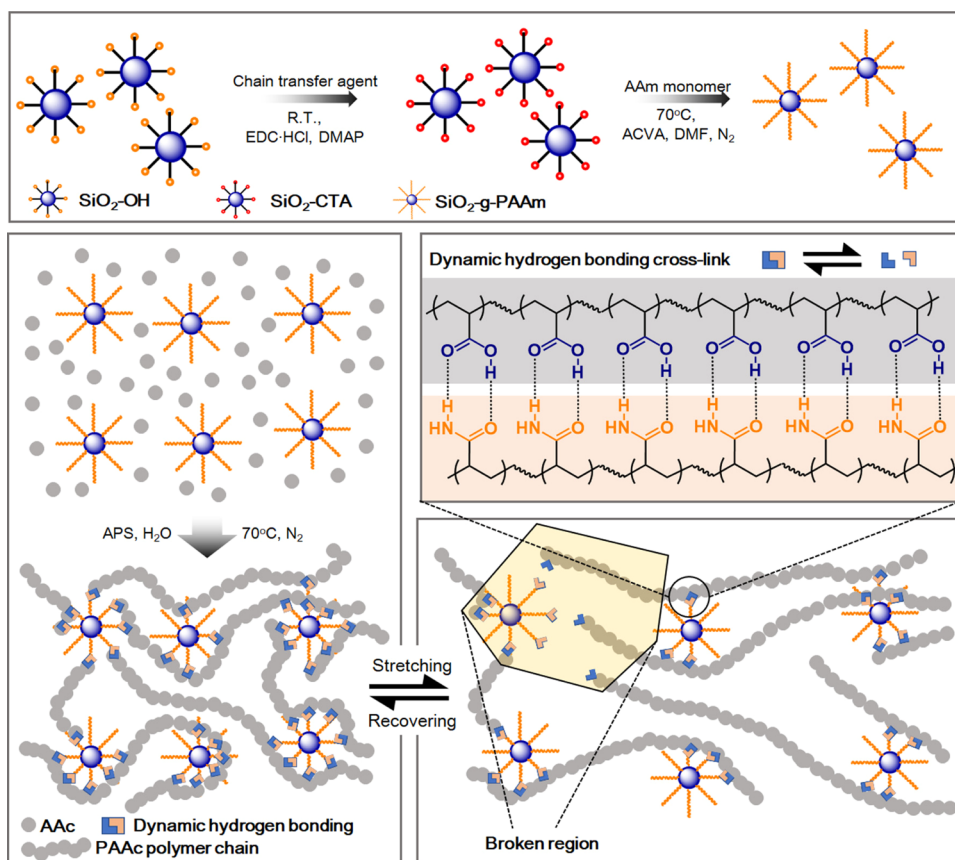
Figure 1. Schematic illustration of preparation of the hybrid nanoparticle SiO$_2$-g-PAAm and the densely dynamic hydrogen bond cross-linked PAAc/SiO$_2$-g-PAAm nanocomposite hydrogel.

simultaneously are highly desirable to meet various practical applications.

In recent years, various strategies have been proposed to fabricate multifunctional hydrogels with the desirable properties as mentioned above. Among them, the most utilized method is introducing the dynamic physical bonds[19−21,30−33] and chemical bonds[13,34−36] into the macromolecular networks together. The reversibility of the dynamic physical bonds endows hydrogels with self-healing capability, whereas the chemical bonds play the role in enhancing their mechanical performance. Although the resulting hydrogels via this method possess self-healing and excellent mechanical strength, they tend to exhibit a lower self-healing efficiency at ambient temperature, and a high self-healing temperature or a long time is generally needed after damage.[20,21] This is because the cross-linkers suppress the mobility of polymer chains, thus resulting in the decrease of the healability of the hydrogels. Meanwhile, most of the self-healing hydrogels as-prepared suffer from a lack of self-adhesiveness, which need additional adhesive tapes or binding straps to be attached onto the human body.[17,27]

A few attempts have been made to construct hydrogels with high mechanical performance and self-healing capability via the combination of multiple physical, noncovalent interactions.[37,38] For example, Zhao et al. recently prepared a hydrogel through integrating hydrogen bonding, electrostatic interactions, and the hydrophobic effect into the polymeric network.[39] Due to the synergistic effect of three noncovalent interactions, the obtained hydrogel exhibited highly stretchable, self-healing, and recoverable properties. However, a long time or a high temperature was needed to achieve the

acceptable self-healing and recoverable efficiency. Duan et al. reported a highly stretchable, tough, and antifatigue hydrogel based on hydrophobic association, ionic bonds, and hydrogen bonds.[40] Although rapid self-recoverable and antifatigue properties were achieved at ambient conditions without external stimuli, the resultant hydrogel suffered from a lack of important self-healing and adhesive properties. Thus, it still remains a challenge to fabricate self-healing hydrogels with excellent self-recovery and adhesive behavior at room temperature without any covalent cross-linkers.

Herein, we propose a simple yet efficient method to prepare highly stretchable, recoverable, self-healing, and adhesive nanocomposite hydrogels using core−shell hybrid nanoparticles SiO$_2$-g-PAAm as a physical cross-linker center (Figure 1). The core−shell particle SiO$_2$-g-PAAm was deliberately designed and synthesized via surface reversible addition−fragmentation chain transfer (RAFT) polymerization of AAm using a SiO$_2$-supported RAFT agent. The inner inorganic core SiO$_2$ with excellent mechanical strength contributed to the improvement of the mechanical performance of the resulting hydrogels. The densely dynamic hydrogen bonds between the outer PAAm chains and PAAc matrices improved the interfacial interactions of SiO$_2$ with PAAc on the one hand and endowed hydrogels with a series of unique properties on the other hand, such as supersoftness, good stretchability, fast recoverability, and self-healing. In addition, the prepared hydrogels exhibited remarkable adhesive properties to diverse substrates, which should be attributed to the abound −COOH and −NH$_2$ groups on PAAc and PAAm. As a result, the PAAc/SiO$_2$-g-PAAm hydrogel-based sensors showed high sensitivity

over a wide range of strains and pressures. Beyond this, the hydrogel-based sensor could accurately monitor various human motions, which would be a reliable candidate for a sensitive human−machine interaction.

2. EXPERIMENTAL METHODS

2.1. Materials. Nanosilica white powders with an average diameter of 30 nm were purchased from Aladdin. 3-Aminopropyl trimethoxysilane, ε-caprolactone, tetrahydrofuran (THF), trichloromethane ($CHCl_3$), dichloromethane (CH_2Cl_2), toluene, ethyl alcohol (EA), 4,4′-azobis(4-cyanovaleric acid) (ACVA), N-3-dimethylaminopropyl-N′-ethyl carbodiimide hydrochloride (EDC·HCl), 4-dimethyl aminopyridine (DMAP), acrylamide (AAm), acrylic acid (AAc), and ammonium persulphate (APS) were purchased from Macklin and used without further purification. Deionized water was produced by a laboratory water maker at 25 °C (18.2 MΩ·cm^{-1} resistivity). All the solvents were dried through a solvent purification system. The chain transfer agent (CTA) S-1-dodecyl-S′-(α,α'-dimethyl-α''-acetic acid) trithiocarbonae (DDAT) was synthesized according to the reported literature.[41]

2.2. Synthesis of the Hydroxyl-Modified Silica Nanoparticles SiO_2−OH. The synthesis of the hydroxyl-modified silica nanoparticles (SiO_2−OH) followed the method we had reported before. At first, the amino-modified silica nanoparticles (SiO_2−NH_2) were synthesized by a coupling reaction. To obtain the homogeneous solution, 3.50 g nanosilica and 200 mL toluene were added into a round-bottom flask and kept stirring for 1 h. Then, 5 mL (3-aminopropyl) trimethoxysilane was added dropwise to the above solution. The mixture was stirred at 90 °C for 6 h. After cooling to room temperature, SiO_2−NH_2 could be collected by centrifugation. Next, 1.23 g SiO_2−NH_2 and 7.51 g ε-caprolactone were dissolved into 200 mL THF. SiO_2−OH was obtained after 12 h of stirring at room temperature followed by centrifugation. All the modified silica nanoparticles were washed with EA three times.

2.3. Synthesis of the SiO_2-Supported RAFT Agent SiO_2-CTA. The macroinitiator SiO_2-CTA was synthesized by the esterification reaction between SiO_2−OH and DDAT. Briefly, 1.33 g SiO_2−OH, 0.56 g CTA, 0.13 g EDC·HCl, and 0.16 g DMAP were added to a round-bottom flask, dissolved in 200 mL $CHCl_3$, and kept stirring for 24 h at room temperature. The product was collected by centrifugation and washed with EA three times. The final product, which was a pale-yellow powder, was dried by freeze-drying and kept in a dry environment for using in the next step.

2.4. Synthesis of the Hybrid Nanoparticle SiO_2-g-PAAm. The hybrid nanoparticle SiO_2-g-PAAm was synthesized via RAFT polymerization using SiO_2-CTA as a macroinitiator. Briefly, 10 g AAm, 1.02 g SiO_2-CTA, and 0.10 g initiator ACVA were added into a Schlenk flask and dissolved in 150 mL DMSO. The mixture was deoxygenated by sparging with nitrogen gas for a period of 30 min. This polymerization was maintained at 70 °C for 6 h under a nitrogen atmosphere. Then, the solution was precipitated into an excess amount of THF and collected by filtration. The obtained SiO_2-g-PAAm was dried to a constant weight under vacuum.

2.5. Preparation of the Nanocomposite Hydrogels PAAc/SiO_2-g-PAAm. The physically cross-linked nanocomposite hydrogels PAAc/SiO_2-g-PAAm were obtained via the polymerization of AA with the as-prepared SiO_2-g-PAAm as a dynamic cross-linker. A typical preparation procedure was described as follows: 0.05 g hybrid nanoparticles SiO_2-g-PAAm were dissolved in 4 mL deionized water followed by ultrasonic dispersion to obtain the homogeneous solution. Next, 0.95 mL AAc and 9.5 mg APS were added to the above solution. Thereafter, the mixed solution was transferred into a tetrafluoroethylene mold (100 × 10 × 2 mm^3). Finally, the hydrogel was obtained after the polymerization reaction that lasted for 12 h at 70 °C in the nitrogen atmosphere. The resulted hydrogel was denoted as PAA/SiO_2-g-PAAm-5%, where 5% refers to the weight ratio of SiO_2-g-PAAm. The PAA/SiO_2-g-PAAm-10% and PAAc/SiO_2-g-PAAm-15% hydrogels were prepared according to the same procedure for the preparation of PAAc/SiO_2-g-PAAm-5%. In

2.6. Characterization. Thermogravimetric analysis (TGA) was performed using a thermal analyzer (TG209F1, NETZSCH, USA) at a heating rate of 10 °C min^{-1} in the nitrogen gas flow. Scanning electron microscopy (SEM) observation was performed with JSM-7500F (JEOL, Japan) at an operation voltage of 5 kV. The samples were freeze-dried. Fourier transform infrared spectra (FT-IR) within the spectra range of 500−4000 cm^{-1} were obtained from a Nicolet 670 spectrometer with the attenuated total reflectance (ATR) accessory. The transmittance of CSH was measured by a UV−vis spectrophotometer (PERSEE ANALYTICS, TU-1901, China).

3. RESULTS AND DISCUSSION

According to the strategy depicted in Figure 1, the multifunctional nanocomposite hydrogels were successfully fabricated using the hybrid nanoparticles SiO_2-g-PAAm as a cross-linker, which were dynamically cross-linked together via the densely dynamic hydrogen bonds between the PAAc matrix and the PAAm chains grafted onto the SiO_2 core. The hybrid nanoparticle acting as a cross-linker was designed using SiO_2 as the core and PAAm as the shell. The SiO_2-supported DDAT as the RAFT agent was synthesized according to the procedure depicted in Scheme S1. First, bare silica reacted with 3-(triethoxysilyl)-propylamin to give the surface amino-modified silica nanoparticles SiO_2−NH_2.[42] Then, the amino groups on the silica surfaces were further converted into hydroxyl groups by reacting with ε-caprolactone. Finally, SiO_2-CTA was obtained as the as-prepared SiO_2−OH that reacted with DDAT via esterification. In order to improve the reaction activity, it was specially designed to attach the DDAT groups onto the SiO_2 surface via a long spacer ($-(CH_2)_3NHCO-(CH_2)_5-$). The successful preparation of SiO_2-CTA was confirmed by FT-IR and TGA techniques. As compared with curve (a) (Figure S1), the peaks in curve (b) at 3130−3700 and 1720 cm^{-1} were attributed to the surface hydroxyl groups and C═O stretching vibration, respectively.[43,44] According to TGA tests (Figure S2), the amount of ε-caprolactone attached to the silica surface was about 4.6%, whereas the amount of DDAT was about 0.6%. The above results confirmed that the macro-RAFT agent SiO_2-CTA was successfully synthesized.

The as-prepared SiO_2-CTA initiated the RAFT polymerization of AAm to produce the hybrid nanoparticles SiO_2-g-PAAm. The weight fraction of the grafted PAAm was determined by TGA, which was about 44% (Figure S2). Then, the physically cross-linked nanocomposite hydrogels PAAc/SiO_2-g-PAAm were obtained via the polymerization of AAc with SiO_2-g-PAAm as a dynamic cross-linker. The resulting hydrogels with 5, 10, and 15% SiO_2-g-PAAm were lyophilized and then broken under liquid nitrogen to observe their morphologies by SEM. From Figure S3, the 3D porous structure could be observed obviously, which is the characteristic structure of the hydrogels. Meanwhile, it can be seen that SiO_2-g-PAAm could be well dispersed in the hydrogel matrix and they formed a uniform network structure that endowed the resultant hydrogels with excellent mechanical properties. In addition, the obtained hydrogels PAAc/SiO_2-g-PAAm exhibited excellent optical transparency, which was over 90% in the full visible region (400−800 nm) (Figure S4). This should be attributed to the homogeneous distribution of the nanoscaled particles SiO_2-g-PAAm in the hydrogels. The intermolecular hydrogen-bonded interaction among the hydrogels was verified via FT-IR (Figure S5) in which the broad absorption peak at 3200−3600 cm^{-1} can be ascribed to the hydrogen bonding between the PAAm and PAAc chains. In
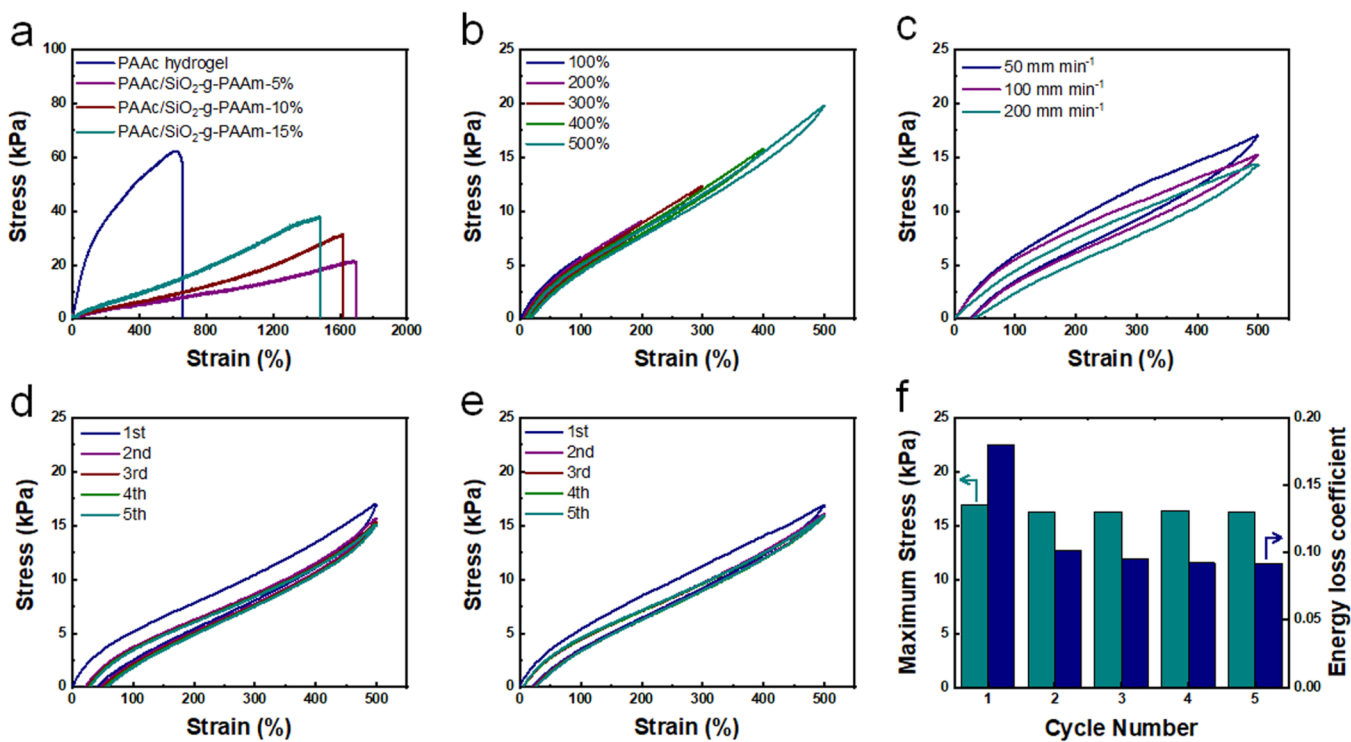
Figure 2. Strength performance of the hydrogels PAAc/SiO$_2$-g-PAAm. Tensile curves of hydrogels containing different SiO$_2$-g-PAAm contents and pure PAAc (a); continuous loading−unloading tensile curves of PAAc/SiO$_2$-g-PAAm-15% at different strains (b); five loading−unloading tensile curves of PAAc/SiO$_2$-g-PAAm-15% at a strain of 500% (d) without any resting time and rest for 1 min (e); and the maximum stress and the energy loss coefficient of PAAc/SiO$_2$-g-PAAm-15% during the five cycling loading−unloading tests (f).
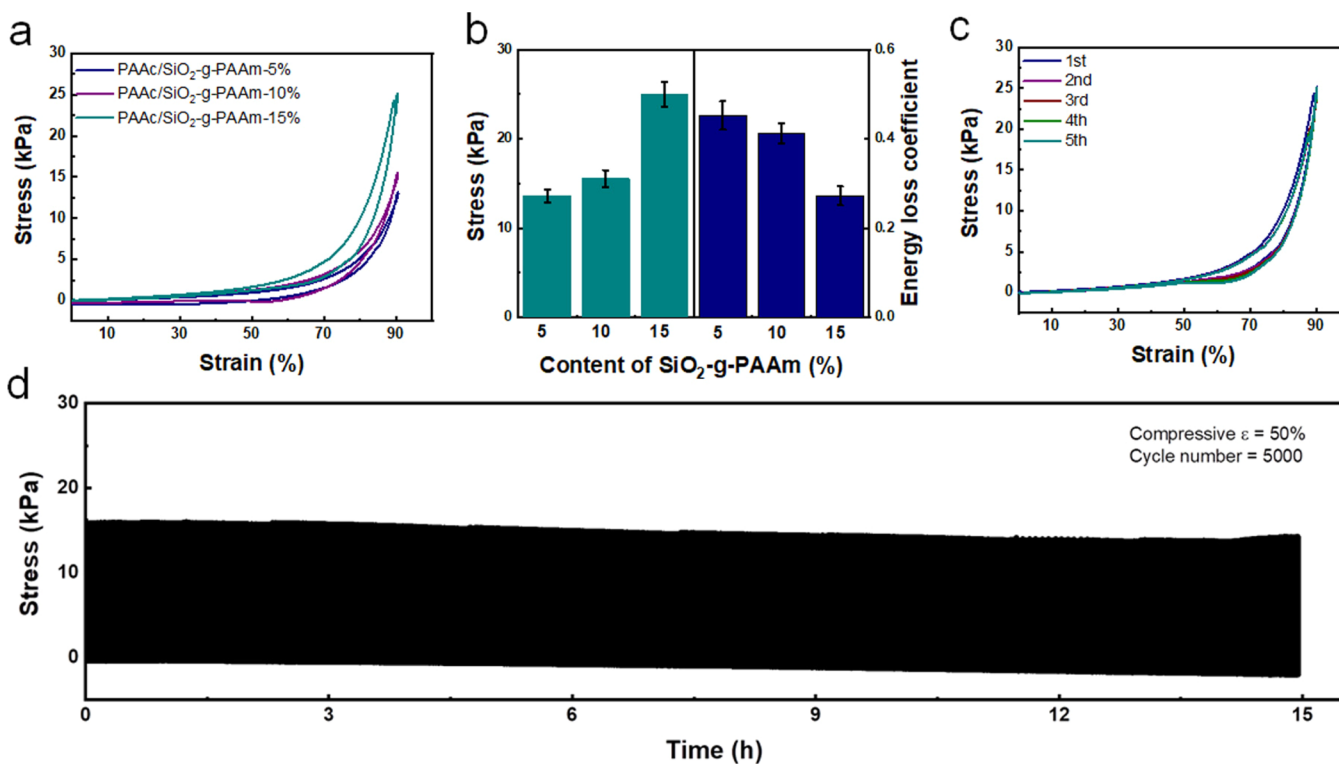

Figure 3. Compressive stress−strain curves of hydrogels with different SiO$_2$-g-PAAm contents at the maximum strain of 90% (a); the column bars of the maximum stress and the ratio of dissipated energy to the loading work of different CSH samples at the maximum strain were 90% (b); continuous loading−unloading compressive curves under 90% strains (c); consecutive 5000 cycles under 50% strains (d).

addition, the peak intensity increased with the increase in the content of SiO$_2$-g-PAAm particles.

The hydrogels PAAc/SiO$_2$-g-PAAm cross-linked via the densely reversible hydrogen bonds exhibited extraordinary
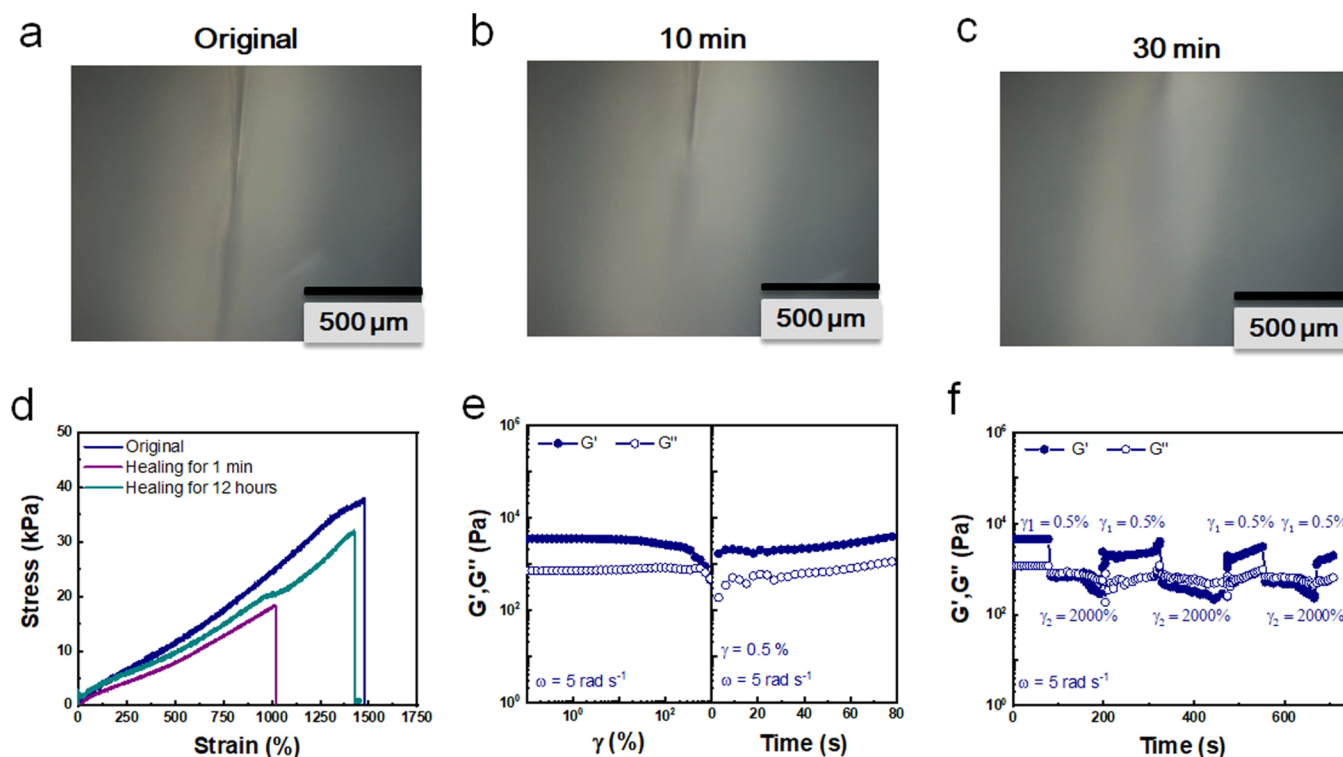
Figure 4. Optical microscopy images of PAAc/SiO$_2$-*g*-PAAm-15% after being sliced for 0 min (a), 10 min (b), and 30 min (c), and the tensile curves of original and healed (healing for 1 min and 12 h at ambient conditions) (d), dynamic alternating strain−time sweep measurement (e), and cyclic shear strain measurement (f).

mechanical properties. The stress−strain curves of the hydrogels with diverse SiO$_2$-*g*-PAAm contents are shown in Figure 2a. Obviously, the tensile properties of the hydrogels were significantly affected by the contents of the SiO$_2$-*g*-PAAm nanoparticles. The fracture stress increased from 19.2 to 34.6 kPa as the SiO$_2$-*g*-PAAm contents increased from 5 to 15%, whereas the fracture strain slightly decreased from 1600 to 1500%. When compared with conventional chemically cross-linked hydrogels, all the samples displayed unique supersoft properties due to the presence of dynamic hydrogen bonds. In addition, these hydrogels were compared with the pure PAAc hydrogel. Although the pure PAAc hydrogel exhibited a higher fracture stress, its elongation obviously decreased. Most importantly, it was the lack of the critical self-healing properties. We further investigated the stability of the prepared hydrogels as being placed under different conditions. As shown in Figure S6, the fracture stress of the hydrogel increased, but the fracture strain decreased with the increase in stored time in air, which was caused by water evaporation. Furthermore, the properties of the hydrogels were also obviously affected by humid conditions, and the important properties of both tensile strain and sensitivity decreased as being placed under 90% RH for 6 h (Figure S7). Thus, the hydrogels are usually coated with a thin layer of silicon oil during the tests to prevent the performance degradation of the electronic devices.

Several tensile cyclic stretching/releasing tests were carried out to examine the energy dissipation mechanism of the hydrogels. At different strain ranges from 100% to 500%, the hydrogels displayed an inconspicuous hysteresis loop in every cycle, indicating the excellent resilience of the prepared hydrogels (Figure 2b). As shown in Figure 2c, both the maximum stress and the hysteresis loop decreased gradually as the tensile speed increased. The reason might be that the

destroyed physically cross-linked structure could undergo partial reconstitution during stretching at lower speed and dissipate more energy. Successive cyclic tensile curves at strains of 500% without any rest time between each cycle are shown in Figure 2d. It was found that the maximum stress slightly decreased from second to fifth cycles, which was obviously less than that of the first cycle, implying that structural changes in the hydrogels occurred during the first cycle, but the same structure was retained in the following cycles. Figure 2e,f shows five-cycle tensile tests employing the same hydrogel with 1 min resting time at room temperature. Obviously, the maximum stress and hysteresis loop were completely recovered and the dissipated energy remained almost constant in the following four cycles after the first cycle. The remarkable self-recovery property was contributed to the dynamically cross-linked bridge structure via the dense hydrogen bonds.

The compressive tests at a strain of 90% were also conducted to investigate the mechanical tolerance and elasticity of the nanocomposite hydrogels PAAc/SiO$_2$-*g*-PAAm. As shown in Figure 3a,b, the hydrogels exhibited excellent compression properties and the compression strength gradually increased with the increase in SiO$_2$-*g*-PAAm content, indicating the effectiveness of SiO$_2$-*g*-PAAm for improving the hydrogel mechanical properties. However, the energy dissipation coefficient decreased with the increase in SiO$_2$-*g*-PAAm content. Meanwhile, it is worth mentioning that when the SiO$_2$-*g*-PAAm content was up to 15%, the maximum stress was only 25 kPa, suggesting that these materials could be employed as the good candidates to fabricate the super-sensitive compressive sensor. Moreover, cyclic compressive loading/unloading tests under a 90% strain were conducted and an obvious overlapping of the cyclic compressive curves appeared after five cycles (Figure 3c). The results indicated
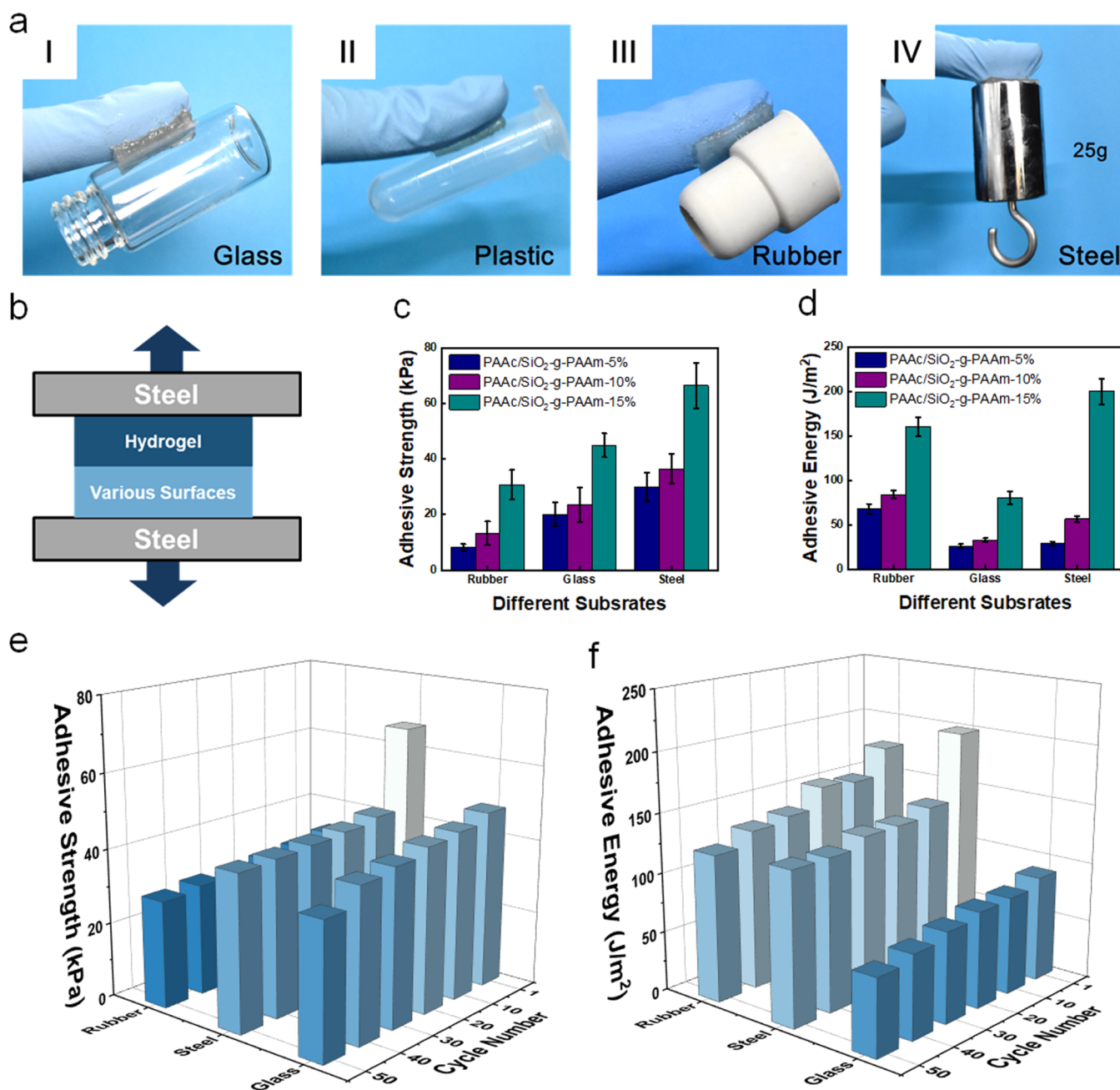
Figure 5. Self-adhesive performance of the PAAc/SiO$_2$-g-PAAm hydrogels. The PAAc/SiO$_2$-g-PAAm hydrogel can adhere to various surfaces (a); schematic of the tensile−adhesive test on adhesion of PAAc/SiO$_2$-g-PAAm (b); the adhesive strength of the hydrogel to different substrates (c); the adhesive energy of the hydrogel to different substrates (d); and repeatable adhesion behavior of the hydrogel to different substrates (e and f).

that the hydrogels PAAc/SiO$_2$-g-PAAm possessed critical parameters of excellent fatigue resistance and rapid self-recovery properties for load-bearing applications. Afterward, 5000 continuous compression cycle tests at a strain of 50% for 15 h were also performed (Figure 3d). The hydrogels PAAc/SiO$_2$-g-PAAm exhibited a nearly unchanged compressive strength throughout the whole procedure, further implying the remarkable elasticity and antifatigue behavior.

Given that the dense hydrogen bonds between the PAAc matrix and PAAm chains grafted on SiO$_2$ can endow the polymer network with superior dynamic reversibility, it is expected that the resulting hydrogels PAAc/SiO$_2$-g-PAAm could be healed efficiently after damage. Optical microscopy images display that the scratch on the sample surface was not

completely seen within 30 mins at ambient conditions, confirming that the sample had very high self-healing efficiency (Figure 4a−c). To further investigate the healing efficiency of hydrogels, the tensile tests were also performed, as shown in Figure 4d. After healing for only 1 min, the recovery of the elongation at break ratio achieved to 68.3%, exhibiting instant healing properties. As the healing time prolonged to 12 h, the ratio recovered to 96.5%. A fast and efficient self-healing performance should be ascribed to the fact that the dynamic hydrogen bonds could dissociate and reform efficiently in a short time.

In addition, oscillatory rheology tests were conducted to investigate the self-repairable behavior of the hydrogel. As shown in Figure 4e, the storage modulus (G') surpassed the
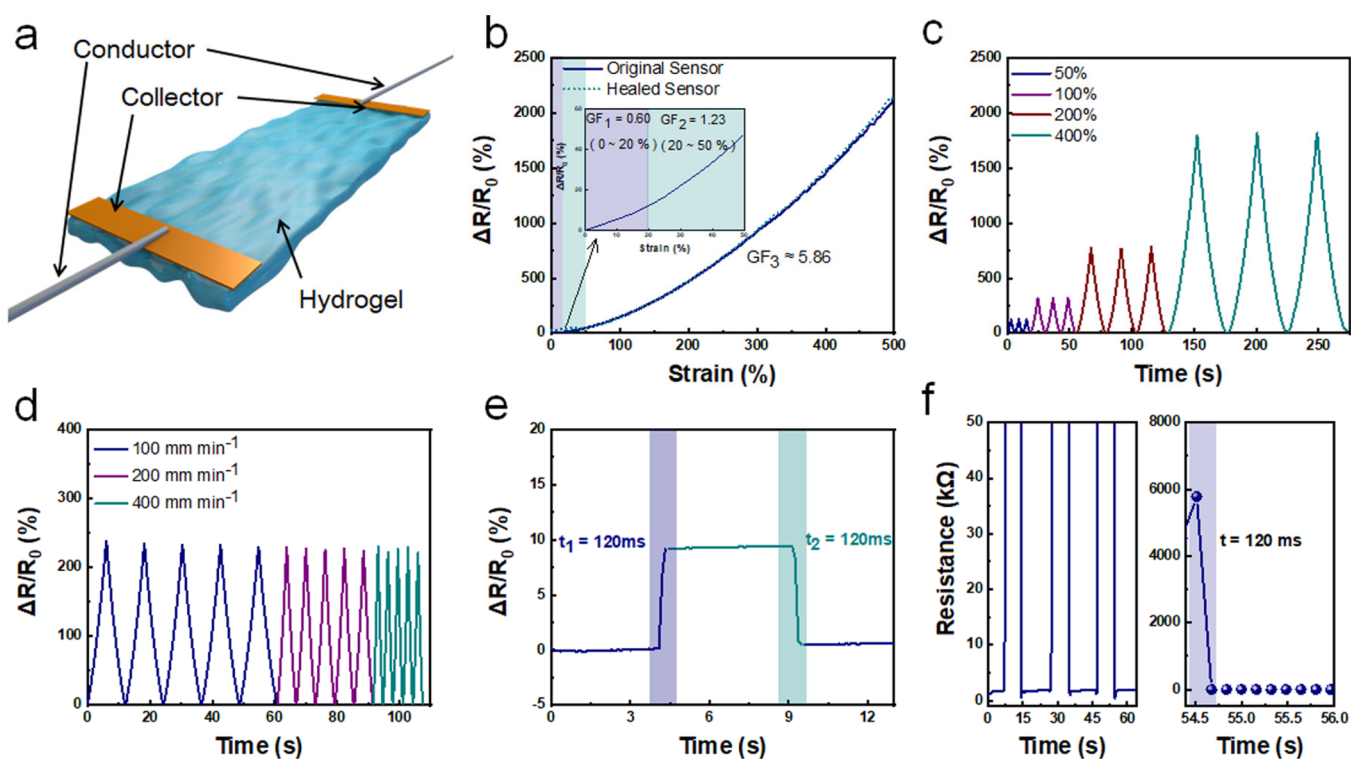
Figure 6. Schematic illustration of the structure of the PAAc/SiO$_2$-g-PAAm hydrogel strain sensor (a); resistance−strain curve of the original sensor and healed sensor (the inset figure shows the resistance changes at 50% strain) (b); cyclic resistance changes over the strain range of 50−400% at a fixed tensile speed of 100 mm min^{-1} (c); relative resistance variation at a strain of 100% with various stretching speeds (d); the response time of the sensor (e); and the self-heal ability tests of the hydrogel-based strain sensor (f).

loss modulus (G'') in a broad strain range, but they cross-linked with the shear strain increasing to about 1000%, indicating the rupture of the hydrogel network. However, the network immediately self-healed once the strain recovered to 0.5%, which was confirmed by the instant and complete recovery of G' and G''. The cyclic experiment with shear strain shifting between 0.5 and 2000% presented the excellent repeatability of the self-healing performance (Figure 4f).

The hydrogels PAAc/SiO$_2$-g-PAAm exhibited another distinctive and advantageous adhesive feature, which can adhere to a broad range of substrates, including organic and inorganic substrates. The strong self-adhesiveness was generated from several possible physical interactions, such as hydrogen bonding (with −OH, −NH$_2$, −CO, N, and O components), metal coordination (with metal ions on the solid surfaces), and van der Waals interaction. As indicated in Figure 5a, the hydrogel could firmly adhere the glove and steel together and easily support a mass of 25 g. The adhesive strength of the hydrogel to the related substrates was quantitatively evaluated by a tensile−adhesion test.[23] From Figure 5c,d, it was observed that the adhesion strength and adhesive energy of the hydrogels were significantly affected toward different substrate surfaces. Among them, the adhesion strength and adhesive energy to iron were the highest, which were ascribed to the synergetic interactions of metal coordination, hydrogen bonds, and van der Waals. In addition, the content of SiO$_2$-g-PAAm could affect the adhesion strength and adhesive energy of the hydrogels. The adhesion strength and adhesive energy on three different substrates were gradually enhanced by increasing the content of SiO$_2$-g-PAAm. The enhancement is likely caused by the increased density of active functional groups. Furthermore, continuous

cyclic adhesion/peel-off tests were conducted to investigate the adhesive antifatigue performance. As demonstrated in Figure 5e,f, the measured adhesion strength and adhesive energy did not almost change even during a longer period for 50 cycles, suggesting their excellent repeatable adhesive capability for practical applications.

The as-prepared hydrogels PAAc/SiO$_2$-g-PAAm exhibited good conductivity because of the substantial amount of water trapped in the polymeric network. As shown in Figure S8, the hydrogel was connected to an electrical circuit to light a light-emitting diode (LED) bulb. It can be seen that the bulb became dim during stretching, whereas it became bright as pressure was applied. This phenomenon demonstrated that the hydrogels were sensitive to variations of strain and pressure. Figure 6a schematically shows the hydrogel electrode for the strain sensor. Figure 6b shows the dependence curve of the relative resistance changes versus the applied strain ranging from 0 to 500%. The gauge factor (GF) was 0.6 in the strain range of 0−20%. As the applied strain increased, GF reached to 1.23 (20−50%) and 5.86 (50−500%), which ensured good sensitivity of the prepared hydrogels. The results shown in Figure 6c further confirmed that the hydrogels possessed good strain sensitivity under the range of 50−400%. During repeated stretching, the relative resistance exhibited excellent repeat-ability under different strains, even at a large strain of 400%, suggesting the excellent conductive stability of the hydrogel. As shown in Figure 6d, the amplitude of the electric resistance signals remained nearly unchanged during the cycles under 100% strain when the deformation rate changed from 100 to 400 mm/min, indicating the excellent frequency tolerance. Moreover, the hydrogel sensor exhibited rapid responsive and recovery behaviors during the pressure loading/unloading
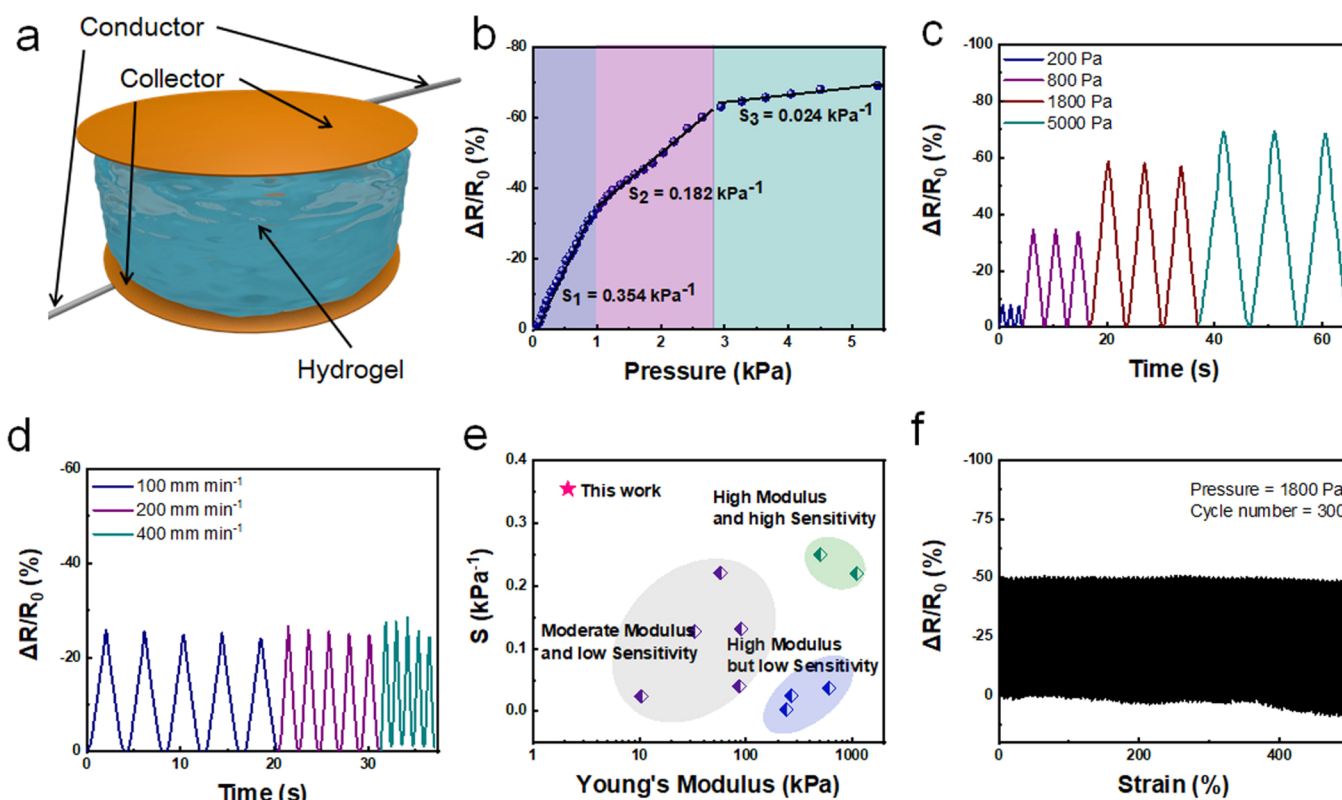
Figure 7. Schematic illustration of the structure of the PAAc/SiO$_2$-*g*-PAAm hydrogel pressure sensor (a); the resistance change as a function of pressure from 0 to 5 kPa (b); cyclic resistance changes over the pressure range of 200−5000 Pa (c); relative resistance variation at a pressure of 800 Pa with various compressing speeds (d); a comparison between this work and previously reported papers (e); and three hundred compressive cycles at a maximum pressure of 1800 Pa (f).

processes under a slight strain of 1%, and both the response time and recovery time were calculated to be 120 ms (Figure 6e). Figure 6f shows the electrical signal change for the hydrogel undergoing three cyclic cutting and self-healing processes. It can be seen that the resistance of the hydrogel could almost repeatedly recover to the original value after the self-healing process, indicating excellent repeatability of the self-repairable electrical property. As shown in Figure 6f, the hydrogel was healed during a very short period of time (0.12 s), suggesting the fast self-healing ability of the hydrogel. Furthermore, the sensor exhibited good reproducibility and durability without no obvious degradation of electric signals during 200 cyclic tensile loading/unloading tests at a strain of 50%, which is significant for the long-term usage of the hydrogel sensors (Figure S9).

In addition to the strain sensing, this PAAc/SiO$_2$-g-PAAm hydrogel could also sense the pressure stimuli. A pressure sensor assembled with the hydrogel is shown in Figure 7a. The resistance−pressure curve is shown in Figure 7b in which the sensitivity could be divided into three regions. When the applied pressure was within the range of 0−1 kPa, the sensitivity was 0.345 kPa^{-1}, which was much higher than the most common hydrogel-based pressure sensor in the literature (Figure 7e).[40,45−54] As the pressure was within the ranges of 1−3 kPa and 3−5 kPa, the sensitivity reached to 0.182 and 0.024 kPa, respectively. Figure 7c indicates that the hydrogel pressure sensor exhibited high sensitivity, and it could respond to the changes of different pressures as being subjected to the repeated compressive loading and unloading procedure. In addition, the relative resistance variation ($\Delta R/R_0$) of the

pressure hydrogel sensor remained almost constant under an applied pressure of 0.8 kPa when the deformation rate changed from 100 to 400 mm/min, and these results indicated that the sensors possessed an outstanding stability (Figure 7d). To investigate the antifatigue performance, 300 cyclic uninterrupted pressure-recovery tests at a pressure of 1.8 kPa were conducted. As demonstrated in Figure 7f, the hydrogel displayed stable and producible response signals, and there was no noticeable shift in the baseline during the cycling test. This excellent antifatigue property should be ascribed to the fast recoverability of the densely dynamic hydrogen bond cross-linked network within the materials. When compared with the reported conductive hydrogels, the prepared hydrogel sensors have not only the higher sensitivity but also possessed the important properties of self-healing and self-adhesiveness (Table S1).

The excellent mechanical properties, self-healing, adhesiveness, high strain and compressive sensitivity, and conductive stability make the nanocomposite hydrogels PAAc/SiO2-g-PAAm ideal potential candidates for the flexible electronic sensors. Moreover, the cytotoxicity test was evaluated by indirect MTT assay and the result revealed that the prepared hydrogels possessed a good biocompatibility, as shown in Figure S10. Thus, the hydrogels were directly attached to different parts of the human body and various real-time motions were monitored via the resistance changes of the hydrogel sensors deriving from a strain or pressure difference. From Figure 8a,b, it can be seen that as the finger bending angles increased from 0 to 90°, the resistance of the hydrogel sensor also rapidly increased, whereas the resistance returned
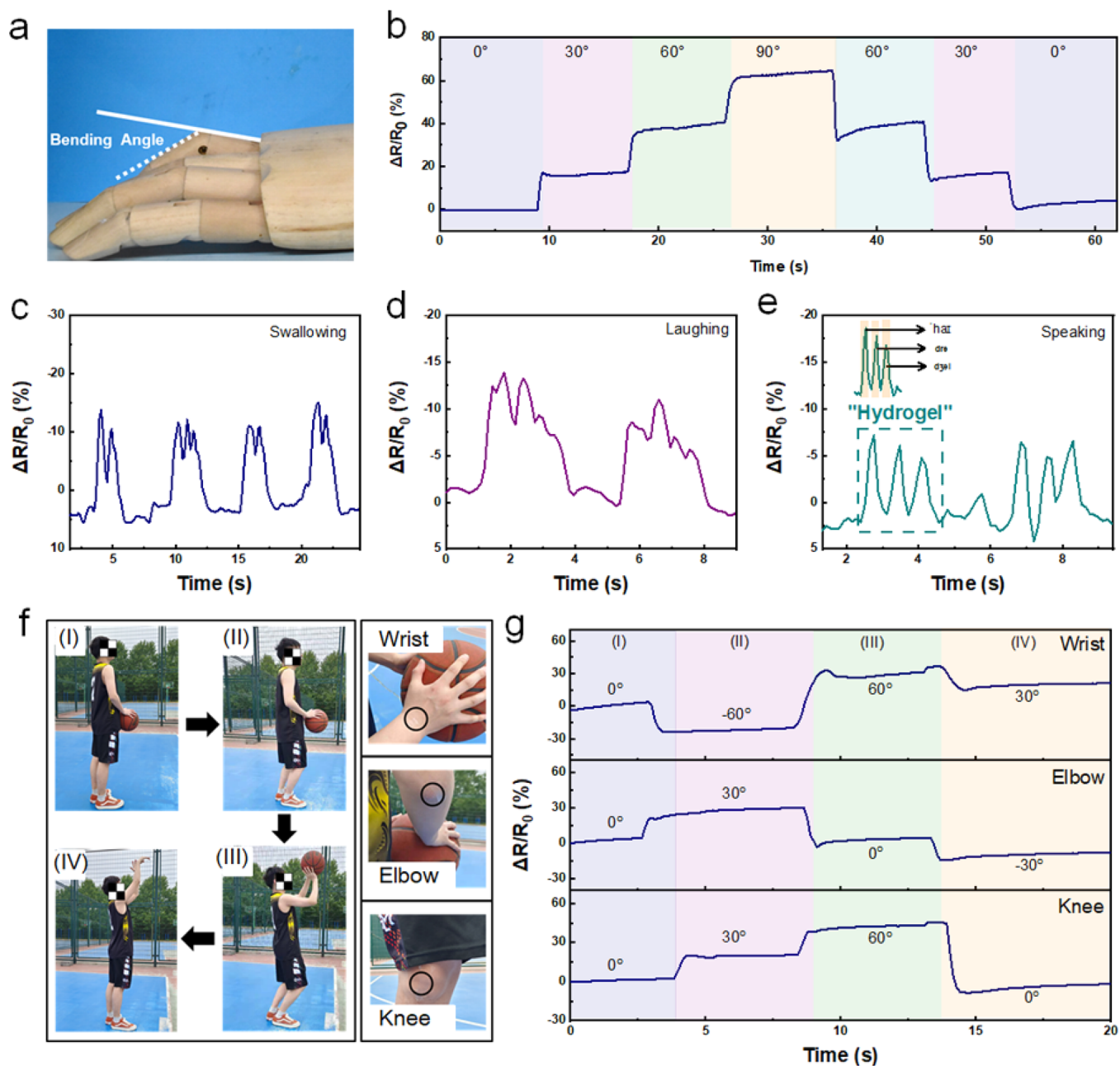
Figure 8. Schematic diagram of the bending angle (a); resistance signals of the hydrogel-based sensor under different finger bending angles (30, 60, and 90°) (b); the relative resistance change of the sensor responding to different deformations at the throat during swallowing (c), laughing (d), and speaking the word of "hydrogel" (e); the relative resistance change of the sensors in one complete basketball shooting behavior as being attached to different positions (f, g).

to the original value when the joint was straightened. The relative resistance variations resulted from the elongation or recovery of the hydrogel as the finger was bent or straightened. In addition, the light body movements with small deformations could also be detected sensitively. The sensor was attached onto a volunteer's neck to detect the throat movement during swallowing, laughing, and speaking (Figure 8c−e). The sensor could record the periodic electrical signals when the volunteer swallowed saliva intermittently. The different output signal patterns could be observed when the volunteer was laughing and speaking. The different three signal peaks in Figure 8e corresponded to the three syllables of the word "hydrogel," including "ˈhaˈhaɪ" "drdrə," and "ddʒelel." Moreover, the

hydrogel-based sensor could monitor continuous and complex human motions depending on the excellent sensitivity and the wide detection range. For example, this sensor could be attached to different joints of the human body to monitor a complete basketball shooting behavior, which had been divided into four steps (labeled as I, II, III, and IV), as illustrated in Figure 8f,g. The real-time electrical signal sensing from the wrist, elbow, and knee would show different waveforms and the maximum response value because the deformation was different in each joint. The above results further confirmed that this hydrogel sensor has promising applications in wearable devices for a wide range of human motion detection.

4. CONCLUSIONS

In this investigation, novel nanocomposite hydrogels combining multiple unique properties were prepared through introducing the hybrid core−shell nanoparticles SiO_2-g-PAAm into the PAAc networks. The hybrid nanoparticles SiO_2-g-PAAm acted as the dynamic cross-linkers to facilitate the hydrogel formation via the dense hydrogen bonds between the long-grafted PAAm chains and the PAAc matrix. The resulting hydrogels exhibited supersoft properties similar to that of human skin and large elongation. Meanwhile, the synergistic interactions of the abound and concentrated hydrogen bonds within the networks endowed the hydrogels with self-healing capability and rapid recoverability at ambient temperature without any external stimuli. In addition, the obtained hydrogels presented an excellent adhesive performance toward different substrates. Moreover, the obtained hydrogel exhibited an excellent adhesive performance that originated from the various functional groups (e.g., $-NH_2$, $-OH$, and $C=O$) and the van der Waals force, which could achieve efficient adhesion at different substrates (e.g., glass, rubber, and steel). The hydrogels were further designed as pressure and strain wearable sensors with outstanding sensitivity and antifatigue properties. The as-prepared sensors could accurately monitor and distinguish both subtle (e.g., swallowing, laughing, and speaking) and large-range human motion (e.g., basketball shooting). Thus, it is believed that this study provides a practical and meaningful approach to fabricate wearable hydrogel sensors with excellent stretchability, fast recoverability, self-healing, and adhesiveness for human healthcare monitoring.

■ ASSOCIATED CONTENT

ⓢ Supporting Information

The Supporting Information is available free of charge at https://pubs.acs.org/doi/10.1021/acs.chemmater.1c01595.

> Fabrication of the hydrogel-based resistance sensor, mechanical measurements, adhesion performance testing, sensing performance and human detection; synthesis of surface hydroxyl group functional silica nanoparticles SiO_2-OH (Scheme S1); summary of the self-healing and self-adhesive properties and sensing performance of different hydrogels (Table S1); and FT-IR spectra, TGA curve of the modified silica, SEM images of different hydrogel samples, UV−vis spectra and FT-IR spectra of the hydrogel, the long-term stability of the hydrogel, photographs of an LED bulb changing when the hydrogel is stretched and compressed, the cyclic loading−unloading tests of the hydrogel-based sensor, and cell viability evaluations of the PAAc/SiO_2-g-PAAm hydrogel (Figures S1−S10) (PDF)

■ AUTHOR INFORMATION

Corresponding Authors

Xiaoshan Fan − *State Key Laboratory for Modification of Chemical Fibers and Polymer Materials, College of Materials Science and Engineering, Innovation Center for Textile Science and Technology, Donghua University, Shanghai 201620, P. R. China;* ⓞ orcid.org/0000-0002-0617-7400; Email: xsfan@dhu.edu.cn

Tianxi Liu − *State Key Laboratory for Modification of Chemical Fibers and Polymer Materials, College of Materials*

Science and Engineering, Innovation Center for Textile Science and Technology, Donghua University, Shanghai 201620, P. R. China; Key Laboratory of Synthetic and Biological Colloids, Ministry of Education, School of Chemical and Material Engineering, Jiangnan University, Wuxi 214122, P. R. China; ⓞ orcid.org/0000-0002-5592-7386; Email: txliu@fudan.edu.cn

Authors

Xiaohui Yu − *State Key Laboratory for Modification of Chemical Fibers and Polymer Materials, College of Materials Science and Engineering, Innovation Center for Textile Science and Technology, Donghua University, Shanghai 201620, P. R. China*

Yong Zheng − *State Key Laboratory for Modification of Chemical Fibers and Polymer Materials, College of Materials Science and Engineering, Innovation Center for Textile Science and Technology, Donghua University, Shanghai 201620, P. R. China*

Haopeng Zhang − *State Key Laboratory for Modification of Chemical Fibers and Polymer Materials, College of Materials Science and Engineering, Innovation Center for Textile Science and Technology, Donghua University, Shanghai 201620, P. R. China*

Yufei Wang − *State Key Laboratory for Modification of Chemical Fibers and Polymer Materials, College of Materials Science and Engineering, Innovation Center for Textile Science and Technology, Donghua University, Shanghai 201620, P. R. China*

Complete contact information is available at:
https://pubs.acs.org/10.1021/acs.chemmater.1c01595

Author Contributions

The manuscript was written through contributions of all authors. All authors have given approval to the final version of the manuscript.

Notes

The authors declare no competing financial interest.

■ ACKNOWLEDGMENTS

■ REFERENCES

(1) Gong, M.; Zhang, L.; Wan, P. Polymer nanocomposite meshes for flexible electronic devices. *Prog. Polym. Sci.* **2020**, *107*, No. 101279.

(2) Chen, X.; Rogers, J. A.; Lacour, S. P.; Hu, W.; Kim, D.-H. Materials chemistry in flexible electronics. *Chem. Soc. Rev.* **2019**, *48*, 1431−1433.

(3) Liu, X. The more and less of electronic-skin sensors. *Science* **2020**, *370*, 910.

(4) Gao, W.; Ota, H.; Kiriya, D.; Takei, K.; Javey, A. Flexible Electronics toward Wearable Sensing. *Acc. Chem. Res.* **2019**, *52*, 523−533.

(5) Bao, Z.; Chen, X. Flexible and Stretchable Devices. *Adv. Mater.* **2016**, *28*, 4177−4179.

(6) Li, X.; Fan, Y. J.; Li, H. Y.; Cao, J. W.; Xiao, Y. C.; Wang, Y.; Liang, F.; Wang, H. L.; Jiang, Y.; Wang, Z. L.; Zhu, G. Ultracomfortable Hierarchical Nanonetwork for Highly Sensitive Pressure Sensor. *ACS Nano* **2020**, *14*, 9605−9612.

(7) Lei, Z.; Wang, Q.; Sun, S.; Zhu, W.; Wu, P. A Bioinspired Mineral Hydrogel as a Self-Healable, Mechanically Adaptable Ionic Skin for Highly Sensitive Pressure Sensing. *Adv. Mater.* **2017**, *29*, No. 1700321.

(8) Zhang, J.; Wan, L.; Gao, Y.; Fang, X.; Lu, T.; Pan, L.; Xuan, F. Highly Stretchable and Self-Healable MXene/Polyvinyl Alcohol Hydrogel Electrode for Wearable Capacitive Electronic Skin. *Adv. Electron. Mater.* **2019**, *5*, No. 1900285.

(9) Amjadi, M.; Kyung, K.-U.; Park, I.; Sitti, M. Stretchable, Skin-Mountable, and Wearable Strain Sensors and Their Potential Applications: A Review. *Adv. Funct. Mater.* **2016**, *26*, 1678−1698.

(10) Hang, C.-Z.; Zhao, X.-F.; Xi, S.-Y.; Shang, Y.-H.; Yuan, K.-P.; Yang, F.; Wang, Q.-G.; Wang, J.-C.; Zhang, D. W.; Lu, H.-L. Highly stretchable and self-healing strain sensors for motion detection in wireless human-machine interface. *Nano Energy* **2020**, *76*, No. 105064.

(11) Shin, J.; Jeong, B.; Kim, J.; Nam, V. B.; Yoon, Y.; Jung, J.; Hong, S.; Lee, H.; Eom, H.; Yeo, J.; Choi, J.; Lee, D.; Ko, S. H. Sensitive Wearable Temperature Sensor with Seamless Monolithic Integration. *Adv. Mater.* **2020**, *32*, No. 1905527.

(12) Fan, H.; Gong, J. P. Fabrication of Bioinspired Hydrogels: Challenges and Opportunities. *Macromolecules* **2020**, *53*, 2769−2782.

(13) Fan, H.; Wang, J.; Jin, Z. Tough, Swelling-Resistant, Self-Healing, and Adhesive Dual-Cross-Linked Hydrogels Based on Polymer−Tannic Acid Multiple Hydrogen Bonds. *Macromolecules* **2018**, *51*, 1696−1705.

(14) Zhang, Y. S.; Khademhosseini, A. Advances in engineering hydrogels. *Science* **2017**, *356*, No. eaaf3627.

(15) Zheng, Y.; Song, H.; Chen, S.; Yu, X.; Zhu, J.; Xu, J.; Zhang, K. A. I.; Zhang, C.; Liu, T. Metal-Free Multi-Heteroatom-Doped Carbon Bifunctional Electrocatalysts Derived from a Covalent Triazine Polymer. *Small* **2020**, *16*, No. 2004342.

(16) Zheng, Y.; Chen, S.; Zhang, K. A. I.; Zhu, J.; Xu, J.; Zhang, C.; Liu, T. Ultrasound-Triggered Assembly of Covalent Triazine Framework for Synthesizing Heteroatom-Doped Carbon Nanoflowers Boosting Metal-Free Bifunctional Electrocatalysis. *ACS Appl. Mater. Interfaces* **2021**, *13*, 13328−13337.

(17) Liu, X.; Liu, J.; Lin, S.; Zhao, X. Hydrogel machines. *Mater. Today* **2020**, *36*, 102−124.

(18) Taylor, D. L.; in het Panhuis, M. Self-Healing Hydrogels. *Adv. Mater.* **2016**, *28*, 9060−9093.

(19) Can, V.; Kochovski, Z.; Reiter, V.; Severin, N.; Siebenbürger, M.; Kent, B.; Just, J.; Rabe, J. P.; Ballauff, M.; Okay, O. Nanostructural Evolution and Self-Healing Mechanism of Micellar Hydrogels. *Macromolecules* **2016**, *49*, 2281−2287.

(20) Yuan, T.; Cui, X.; Liu, X.; Qu, X.; Sun, J. Highly Tough, Stretchable, Self-Healing, and Recyclable Hydrogels Reinforced by in Situ-Formed Polyelectrolyte Complex Nanoparticles. *Macromolecules* **2019**, *52*, 3141−3149.

(21) Long, T.; Li, Y.; Fang, X.; Sun, J. Salt-Mediated Polyampholyte Hydrogels with High Mechanical Strength, Excellent Self-Healing Property, and Satisfactory Electrical Conductivity. *Adv. Funct. Mater.* **2018**, *28*, No. 1804416.

(22) Chen, W.-P.; Hao, D.-Z.; Hao, W.-J.; Guo, X.-L.; Jiang, L. Hydrogel with Ultrafast Self-Healing Property Both in Air and Underwater. *ACS Appl. Mater. Interfaces* **2018**, *10*, 1258−1265.

(23) Jung, H.; Kim, M. K.; Lee, J. Y.; Choi, S. W.; Kim, J. Adhesive Hydrogel Patch with Enhanced Strength and Adhesiveness to Skin for Transdermal Drug Delivery. *Adv. Funct. Mater.* **2020**, *30*, No. 2004407.

(24) Yang, J.; Bai, R.; Suo, Z. Topological Adhesion of Wet Materials. *Adv. Mater.* **2018**, *30*, No. 1800671.

(25) Hao, S.; Shao, C.; Meng, L.; Cui, C.; Xu, F.; Yang, J. Tannic Acid−Silver Dual Catalysis Induced Rapid Polymerization of Conductive Hydrogel Sensors with Excellent Stretchability, Self-Adhesion, and Strain-Sensitivity Properties. *ACS Appl. Mater. Interfaces* **2020**, *12*, 56509−56521.

(26) Yang, J.; Steck, J.; Bai, R.; Suo, Z. Topological adhesion II. Stretchable adhesion. *Extreme Mech. Lett.* **2020**, *40*, No. 100891.

(27) Xie, C.; Wang, X.; He, H.; Ding, Y.; Lu, X. Mussel-Inspired Hydrogels for Self-Adhesive Bioelectronics. *Adv. Funct. Mater.* **2020**, *30*, No. 1909954.

(28) Mao, J.; Zhao, C.; Liu, L.; Li, Y.; Xiang, D.; Wu, Y.; Li, H. Adhesive, transparent, stretchable, and strain-sensitive hydrogel as flexible strain sensor. *Compos. Commun.* **2021**, *25*, No. 100733.

(29) Wu, L.; Hu, Y.; Tang, P.; Wang, H.; Bin, Y. High stretchable, pH-sensitive and self-adhesive rGO/CMCNa/PAA composite conductive hydrogel with good strain-sensing performance. *Compos. Commun.* **2021**, *24*, No. 100669.

(30) Zhao, Z.; Zhuo, S.; Fang, R.; Zhang, L.; Zhou, X.; Xu, Y.; Zhang, J.; Dong, Z.; Jiang, L.; Liu, M. Dual-Programmable Shape-Morphing and Self-Healing Organohydrogels Through Orthogonal Supramolecular Heteronetworks. *Adv. Mater.* **2018**, *30*, No. 1804435.

(31) Hong, S. H.; Kim, S.; Park, J. P.; Shin, M.; Kim, K.; Ryu, J. H.; Lee, H. Dynamic Bonds between Boronic Acid and Alginate: Hydrogels with Stretchable, Self-Healing, Stimuli-Responsive, Remoldable, and Adhesive Properties. *Biomacromolecules* **2018**, *19*, 2053−2061.

(32) Andersen, A.; Krogsgaard, M.; Birkedal, H. Mussel-Inspired Self-Healing Double-Cross-Linked Hydrogels by Controlled Combination of Metal Coordination and Covalent Cross-Linking. *Biomacromolecules* **2018**, *19*, 1402−1409.

(33) Xu, K.; Wang, Y.; Zhang, B.; Zhang, C.; Liu, T. Stretchable and self-healing polyvinyl alcohol/cellulose nanofiber nanocomposite hydrogels for strain sensors with high sensitivity and linearity. *Compos. Commun.* **2021**, *24*, No. 100677.

(34) Guo, H.; Hong, W.; Kurokawa, T.; Matsuda, T.; Wu, Z. L.; Nakajima, T.; Takahata, M.; Sun, T.; Rao, P.; Gong, J. P. Internal Damage Evolution in Double-Network Hydrogels Studied by Microelectrode Technique. *Macromolecules* **2019**, *52*, 7114−7122.

(35) Khiêm, V. N.; Mai, T.-T.; Urayama, K.; Gong, J. P.; Itskov, M. A Multiaxial Theory of Double Network Hydrogels. *Macromolecules* **2019**, *52*, 5937−5947.

(36) Yang, M.; Liu, C.; Li, Z.; Gao, G.; Liu, F. Temperature-Responsive Properties of Poly(acrylic acid-co-acrylamide) Hydrophobic Association Hydrogels with High Mechanical Strength. *Macromolecules* **2010**, *43*, 10645−10651.

(37) Wang, Z.; An, G.; Zhu, Y.; Liu, X.; Chen, Y.; Wu, H.; Wang, Y.; Shi, X.; Mao, C. 3D-printable self-healing and mechanically reinforced hydrogels with host−guest non-covalent interactions integrated into covalently linked networks. *Mater. Horiz.* **2019**, *6*, 733−742.

(38) Clarke, D. E.; Pashuck, E. T.; Bertazzo, S.; Weaver, J. V. M.; Stevens, M. M. Self-Healing, Self-Assembled β-Sheet Peptide−Poly(γ-glutamic acid) Hybrid Hydrogels. *J. Am. Chem. Soc.* **2017**, *139*, 7250−7255.

(39) Zhao, B.; Jiang, H.; Lin, Z.; Xu, S.; Xie, J.; Zhang, A. Preparation of acrylamide/acrylic acid cellulose hydrogels for the adsorption of heavy metal ions. *Carbohydr. Polym.* **2019**, *224*, No. 115022.

(40) Xia, S.; Zhang, Q.; Song, S.; Duan, L.; Gao, G. Bioinspired Dynamic Cross-Linking Hydrogel Sensors with Skin-like Strain and Pressure Sensing Behaviors. *Chem. Mater.* **2019**, *31*, 9522−9531.

(41) Cheng, H.; Fan, X.; Wang, X.; Ye, E.; Loh, X. J.; Li, Z.; Wu, Y.-L. Hierarchically Self-Assembled Supramolecular Host−Guest Delivery System for Drug Resistant Cancer Therapy. *Biomacromolecules* **2018**, *19*, 1926−1938.

(42) Liu, S.; Fan, X.; He, C. Improving the fracture toughness of epoxy with nanosilica-rubber core-shell nanoparticles. *Compos. Sci. Technol.* **2016**, *125*, 132−140.

(43) Zhang, X.; Sheng, N.; Wang, L.; Tan, Y.; Liu, C.; Xia, Y.; Nie, Z.; Sui, K. Supramolecular nanofibrillar hydrogels as highly stretchable, elastic and sensitive ionic sensors. *Mater. Horiz.* **2019**, *6*, 326−333.

(44) Wang, Y. J.; Zhang, X. N.; Song, Y.; Zhao, Y.; Chen, L.; Su, F.; Li, L.; Wu, Z. L.; Zheng, Q. Ultrastiff and Tough Supramolecular Hydrogels with a Dense and Robust Hydrogen Bond Network. *Chem. Mater.* **2019**, *31*, 1430−1440.

(45) He, F.; You, X.; Gong, H.; Yang, Y.; Bai, T.; Wang, W.; Guo, W.; Liu, X.; Ye, M. Stretchable, Biocompatible, and Multifunctional Silk Fibroin-Based Hydrogels toward Wearable Strain/Pressure Sensors and Triboelectric Nanogenerators. *ACS Appl. Mater. Interfaces* **2020**, *12*, 6442−6450.

(46) Qin, Z.; Sun, X.; Yu, Q.; Zhang, H.; Wu, X.; Yao, M.; Liu, W.; Yao, F.; Li, J. Carbon Nanotubes/Hydrophobically Associated Hydrogels as Ultrastretchable, Highly Sensitive, Stable Strain, and Pressure Sensors. *ACS Appl. Mater. Interfaces* **2020**, *12*, 4944−4953.

(47) Liu, X.; Zhang, Q.; Gao, G. Solvent-Resistant and Nonswellable Hydrogel Conductor toward Mechanical Perception in Diverse Liquid Media. *ACS Nano* **2020**, *14*, 13709−13717.

(48) Fu, X.; Li, J.; Tang, C.; Xie, S.; Sun, X.; Wang, B.; Peng, H. Hydrogel Cryo-Microtomy Continuously Making Soft Electronic Devices. *Adv. Funct. Mater.* **2021**, *31*, No. 2008355.

(49) Ye, Y.; Zhang, Y.; Chen, Y.; Han, X.; Jiang, F. Cellulose Nanofibrils Enhanced, Strong, Stretchable, Freezing-Tolerant Ionic Conductive Organohydrogel for Multi-Functional Sensors. *Adv. Funct. Mater.* **2020**, *30*, No. 2003430.

(50) Zhang, Q.; Liu, X.; Ren, X.; Jia, F.; Duan, L.; Gao, G. Nucleotide-Regulated Tough and Rapidly Self-Recoverable Hydrogels for Highly Sensitive and Durable Pressure and Strain Sensors. *Chem. Mater.* **2019**, *31*, 5881−5889.

(51) Wu, M.; Chen, J.; Ma, Y.; Yan, B.; Pan, M.; Peng, Q.; Wang, W.; Han, L.; Liu, J.; Zeng, H. Ultra elastic, stretchable, self-healing conductive hydrogels with tunable optical properties for highly sensitive soft electronic sensors. *J. Mater. Chem. A* **2020**, *8*, 24718−24733.

(52) Yu, J.; Dang, C.; Liu, H.; Wang, M.; Feng, X.; Zhang, C.; Kang, J.; Qi, H. Highly Strong and Transparent Ionic Conductive Hydrogel as Multifunctional Sensors. *Macromol. Mater. Eng.* **2020**, *305*, No. 2000475.

(53) Liu, X.; Yu, L.; Zhu, Z.; Nie, Y.; Skov, A. L. Silicone-Ionic Liquid Elastomer Composite with Keratin as Reinforcing Agent Utilized as Pressure Sensor. *Macromol. Rapid Commun.* **2021**, *42*, No. 2000602.

(54) Sun, X.; Yao, F.; Wang, C.; Qin, Z.; Zhang, H.; Yu, Q.; Zhang, H.; Dong, X.; Wei, Y.; Li, J. Ionically Conductive Hydrogel with Fast Self-Recovery and Low Residual Strain as Strain and Pressure Sensors. *Macromol. Rapid Commun.* **2020**, *41*, No. 2000185.